DOI: 10.1002/smll.200700368

Fast Mass Transport Through Carbon Nanotube Membranes

Henk Verweij, Melissa C. Schillo, and Ju Li*

The May 19, 2006 issue of Science included a paper by Holt et al.[1] on "Fast Mass Transport Through Sub-2-Nanometer Carbon Nanotubes". The paper was also featured on the cover, showing methane molecules translating inside a carbon nanotube (CNT). The authors explained how they prepared 2–6-μm thin membranes consisting of double-walled carbon nanotubes (DWNTs) all aligned perpendicular to the apparent membrane surface. These tubes are open at both ends and the space between the tubes is filled with dense Si_3N_4. Pure gas and water fluxes were measured at room temperature with the application of a small pressure difference. Interpretation of the results led to the conclusion that the membranes showed much higher fluxes than what was estimated from Knudsen gas diffusion and Poiseuille viscous flow models. The membranes have a straight-channel morphology with a narrow pore-size distribution and exceptionally smooth pore walls. The unusual geometry and surface properties make it difficult to compare the membrane's properties with common membranes but there is no question that the mass transport in the aligned DWNTs is fast indeed. To appreciate how fast, we will consider their transport properties starting from the perspective of "conventional" porous membrane technology. Recent molecular dynamics simulations suggest that none of the classic models for gas (Knudsen) and water (Poiseuille) permeation work in a meaningful way for these nanotube membranes, and new models are needed.

Keywords:
- carbon nanotubes
- diffusion
- membranes
- molecular dynamics
- viscous flow

1. Introduction

Membrane technology provides opportunities to conduct important separations with minimal use of energy (dissipation). For the sake of simplicity we will mostly consider the case of a single species, l_1, that can permeate easily through the membrane. Separation of these species from mixtures occurs because other components, l_2, are partly or completely blocked by the membrane. One of the most well-known membrane separations is *filtration* of particles dispersed in a fluid (gas or liquid). The membrane is in that case a filter plate with holes (pores) that are too small for the particles, l_2, to pass, but big enough for the fluid (gas, liquid), l_1, to permeate easily. This separation principle is know as *size exclusion* and occurs at any length scale, from freight wagons that pass a tunnel, tulip bulbs classified on a perforated plate, to >0.4 nm hydrocarbon molecules that are blocked by an amorphous silica membrane with <0.4 nm pores.[2]

For the <100 nm length scale, separation principles other than size exclusion exist, which are based on a certain physical interaction with the membrane materials. Examples include prevailing collision of molecules with the pore wall (Knudsen diffusion), trapping of mobile molecules in an at-

[*] Prof. H. Verweij, M. C. Schillo, Prof. J. Li
Department of Materials Science & Engineering
Ohio State University
2041 N College Road, Columbus OH 43210-1178 (USA)
Fax: (+1) (614)-292-7427
E-mail: verweij.1@osu.edu

tractive pore wall potential well (diffusion), and space charge effects induced by charged pore walls (ionic nanofiltration).

Permeation of a molecule through an *ideally permeable* membrane occurs without energy dissipation. If chemical equilibrium is reached, gaseous molecules have about the same partial pressure at both sides of the membrane; liquids experience isostatic pressures that differ by the osmotic value. Real membranes require a substantial driving force, most generally expressed as a gradient in chemical potential. Real membrane transport is dissipative and often not 100% selective for just one species. The selectivity of membranes is generally optimized for a target separation by choosing a certain microstructure and chemical composition. The dissipative resistance of the membranes can be diminished by making the membranes as thin as possible on a smooth and strong, but permeable support structure. However, decreasing the membrane thickness increases the risk of selectivity loss by pinholes with a pore diameter, $Ø_p$, much larger than the designed diameter. In addition, there is a possibility that surface transfer kinetics start to determine overall membrane resistance.

2. DWNT Membrane Manufacturing

The experiments described by Holt et al.[1] were built upon earlier studies[3] of the manufacturing and properties of aligned multi-walled carbon nanotubes (MWNTs). These tubes were 5–10 μm long with $Ø_p = 20$–50 nm, and their area densities were typically 4×10^{10} NT tips per cm^2. However, the preparation of highly permeable MWNT membranes was found to be hindered by the formation of impermeable "bamboo knot" obstructions and blocking by catalyst particles. This led Holt et al. to decide to focus on membranes of aligned single-wall and, in particular, DWNTs with $Ø_p = 1$–2 nm. Their fabrication route was similar to that of an earlier report,[3] and is shown in Figure 1. The process started with a test grade Si(100) wafer coated with ≈250 nm of low-stress silicon nitride grown by low-pressure chemical vapor deposition (LPCVD). KOH etching formed microscale pits on a 2×2 cm device and produced an array of 89 pits of 700×700 μm lateral dimension. A 50-μm-thick silicon layer was left, initially, on the side opposite to the pits. Hydrofluoric acid (HF) etching removed the initial silicon nitride and exposed the silicon surface. A multilayer catalyst precursor of 10 nm Al, 0.3 nm Mo, and 0.5 nm Fe was deposited by electron-beam deposition, followed by annealing at 850 °C at 0.1 MPa total pressure, maintained with 600 sccm Ar and 400 sccm H_2. This resulted in a break-up of the catalyst multilayer into a dense array of nanoparticles. The nanoparticles catalyze the formation of DWNTs in the presence of 100 sccm ethylene at 850 °C.

Since fluid flow is only desired through the internal pore, impermeable Si_3N_4 was deposited on and between the tubes by LPCVD at 805 °C. Si_3N_4 was also chosen because of its mechanical support capability as well as its ability to conform around the tubes. Si_3N_4 deposition was followed by exposure to XeF_2 to etch away the 50 μm Si layer beneath the membrane to expose the membrane back. In each of the 89 pits, the exposed membrane had a 50 μm diameter, which corresponds to an overall exposed membrane area of 1.7×10^{-3} cm^2. Argon ion-beam etching and O_2 reactive ion etching were used to remove excess Si_3N_4, metallic nanoparticles, and the nanotube end caps.

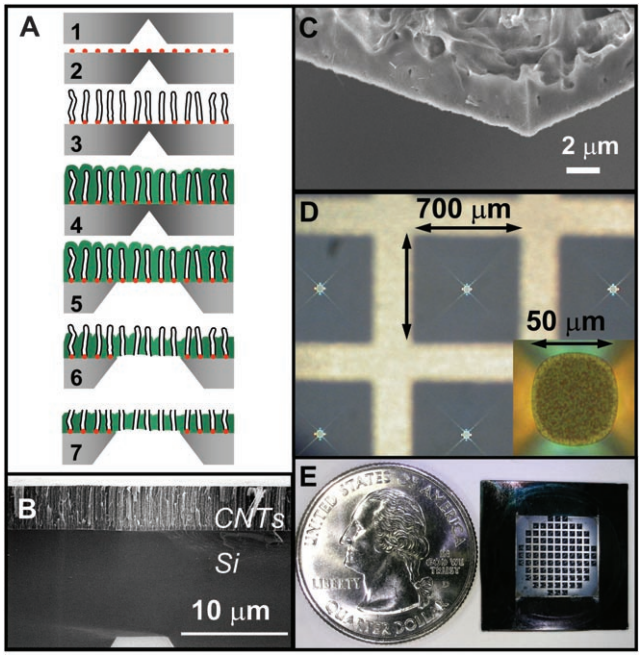

Figure 1. A) DWNT membrane fabrication process; B) SEM cross section of DWNTs; C) SEM cross section of the membrane: silicon nitride matrix around CNTs; D) photograph of open membrane areas; the inset is a close up of one membrane; E) photograph of a membrane chip with 89 windows. Reproduced with permission.[1]

3. Characteristic Numbers and Definitions

Membrane performance is often expressed in terms of the *permeance*, f, of species l_1, and the *selectivity*, α, with respect to another species, l_2. Membrane gas-transport parameters are obtained for individual layers, or as an overall quantity, f^{tot} or α^{tot}, for a multilayer-supported membrane structure. The permeance is often used for structures where the effective membrane layer thickness is unknown. In addition, it can be useful in comparisons of the transport resistance of individual layers. Holt et al.[1] expressed membrane transport in terms of volumetric flow through 50-μm-diameter areas of perpendicularly aligned nanotubes. Note that the permeability in Figure 4 of their 2006 paper[1] is actually a permeance; an unambiguous comparison requires a correction for the thickness values in Table 2 of that article.[1] To facilitate comparison with other membrane studies we use SI units and provide, in the next paragraphs, a number of definitions that are common in the inorganic membrane community.

Gas flow, n, is expressed unambiguously as moles per second. The molar flux, j, is the flow per unit of area, A,

perpendicular to the flow. The molar permeance (or permeation), f, is the stationary flux, normalized for pressure difference, Δp. The molar permeability, k, is the permeance, normalized for thickness. The actual molecular selectivity, α_{l_1,l_2}, of individual layers is the ratio of gas permeances measured for mixtures that differ in composition at the feed, f, and the permeate, p, side. Practical values of α_{l_1,l_2} are often calculated from steady-state average composition ratios. However, this value can deviate from the true membrane selectivity because of mass-transfer limitation in the boundary layers near the feed and permeate surfaces. It is for this reason that molecular selectivity is often expressed as permselectivity (or ideal selectivity), $\alpha^s_{l_1l_2}$. This is the ratio of the single gas permeances of l_1 with respect to l_2, measured under the same conditions. $\alpha^s_{l_1l_2}$ does not account for interaction between species inside the membrane.

For liquids, it is more convenient to use the volumetric flow, n_ℓ, expressed as $m^3 s^{-1}$. The mechanical permeance, f_ℓ, is the stationary flux, j_ℓ, normalized for dynamic viscosity, η_ℓ, and pressure difference. The mechanical permeability, k_ℓ, is the mechanical permeance, normalized for thickness. The selectivity in liquid separation is expressed in terms of retention or rejection, $R_l = 1 - c_p/c_f$ where c_p and c_f are the concentrations of permeate and feed, respectively.

To further quantify the performance of DWNT membranes with respect to other membranes, a number of quantitative expressions are provided for the most relevant transport regimes of membrane permeance.

4. Transport Mechanisms: Expressions

The transport of the permeating species depends strongly on the membrane pore diameter $\emptyset_p$ and the interaction of that species with the membrane structure. Porous membranes are classified by using IUPAC terminology[4] that stems from gas sorption analysis. Accessible micropores have $\emptyset_p < 2$ nm; mesopores have $2 < \emptyset_p < 50$ nm, and macropores have $\emptyset_p > 50$ nm. This classification also provides approximate boundaries for different transport (and separation) mechanisms that are relevant for gases and liquids, as summarized in Table 1.

4.1. Micropore Transport

Micropore diameters are in the molecular size range, where any distinction between aggregation states (gas, liquid) ceases to exist. The molecules feel the interaction potential of the pore wall and their transport can be described in terms of hopping diffusion like a solid-state vacancy mechanism. This mechanism applies in particular for amorphous structures and molecules that fit tightly in the pore. The membrane pore system can then be considered as a Langmuir lattice of sites that can be either vacant or occupied by molecules. For that case a generic expression for the flux of l_1 in a binary mixture is[5]

$$j_{l_1} = -\tilde{f}_{L,l_1} b^0_{l_1} c^{tot} RT\left[(1-\theta_{l_2})\nabla\theta_{l_1} + \theta_{l_1}\nabla\theta_{l_2}\right] \quad (1)$$

in which b^0 is the mechanical mobility for a molecule on an otherwise empty lattice, c^{tot} the concentration of available sites, RT is the product of the universal gas constant and absolute temperature, and $0 < \theta < 1$ is the average site occupation. Boundary conditions for Equation (1) can be obtained from expressions for the chemical equilibrium with the fluid at the membrane feed and permeate. The non-equilibrium correlation factor, $0 < \tilde{f}_{L,l_1} < 1$ is often very close to 1, but can become very small for mobile molecules with low θ that percolate on a micropore network that is also occupied by slower molecules with high θ. This leads to the distinction of two types of microporous or surface diffusion separation:[5]

Type 1: Both molecules have little affinity and hence $\theta \to 0$. This type of behavior is often found for small gas molecules, low pressures, and high temperatures. It results in significant simplification of Equation (1) so that $\alpha_{l_1l_2} = \alpha^s_{l_1l_2}$ in the absence of external mass-transfer limitations.

Type 2: One of the molecules has a much higher affinity (and hence lower mobility). It may occupy $>50\%$ of the sites and form a percolative network, nearly impermeable for the other molecule.

Type 1 behavior leads to a very simple expression for the diffusion flux for individual species l:

$$j_l = -b^0_l c^{tot} RT\nabla\theta_l = -\tilde{D}_l \nabla c_l \quad (2)$$

Table 1. Pore size versus transport regimes for gases and liquids. Note that this is a very generic classification. Each individual case needs further detailed analysis. Simple size exclusion (SE) is not considered in this table.

Pore size	Gas			Liquid		
	Permeation	Separation	Characteristic length	Permeation	Separation	Characteristic length
Microporous: $\emptyset_p < 2$ nm	Constrained molecular diffusion	Mobility, concentration differences	Range pore wall interaction potential; kinetic diameter molecule	Constrained molecular diffusion, surface transfer	Mobility, concentration differences	Range pore wall interaction potential; kinetic diameter molecule
Mesoporous: $2 < \emptyset_p < 50$ nm	Knudsen diffusion	Thermalized kinetic energy	Mean free path length molecules in bulk gas	Viscous flow	Ion retention by charged pore walls	Debye length
Macroporous: $\emptyset_p > 50$ nm	Viscous flow (bulk diffusion)	None	Flow field around particle (for SE)	Viscous flow (bulk diffusion)	None	Flow field around particle (for SE)

which is Fick's first law for a single species with the chemical diffusion coefficient $\tilde{D}_l = b_l^0 RT$, independent of θ. In type 1 behavior, the Henry isotherm, $\theta_l = K_l^H p_l / p^0$, may be applicable so that the diffusion permeance is obtained in that case, independent of p_l as

$$f_j^1 = \frac{b_l^0 c^{\text{tot}} \mathrm{R}T \nabla \theta_l}{(p_{l,\text{f}} - p_{l,\text{p}})} = \frac{c^{\text{tot}} \tilde{D}_l K_l^H}{p^0 X} \tag{3}$$

in which p^0 is a standard pressure and X is the apparent membrane thickness. For the DWNTs the hopping diffusion is not applicable and must be replaced by a kinetic model. However, there is a striking similarity between type 2 hopping permeation and the kinetic mechanism at high concentrations. All this is discussed in much more detail in Section 5.

4.2. Gas-Phase Transport by Knudsen Diffusion

The transport of gases in mesopores generally occurs by the Knudsen diffusion mechanism if the mean free path length of the molecules is larger than the pore diameter. This means that the molecules collide with the pore wall before they collide with each other. Each collision occurs with complete *thermalization* so that the angle of reflection is fully randomized with respect to the angle of incidence. The Knudsen permeance is driven by a particle density (concentration) difference and is largely independent of p_j as is the case for type 1 microporous transport

$$f_l^{\text{Kn}} = \frac{\phi_\text{p} \varnothing_\text{p}}{3\tau X} \sqrt{\left(\frac{8}{\pi \mathrm{R}T M_l}\right)} \tag{4}$$

in which ϕ_p is the volume fraction of porosity, τ is the average tortuosity of the pores, and M is the molar mass. The Knudsen mechanism is only slightly separative with a theoretical separation factor $\alpha_{l_1,l_2}^{Kn} = \sqrt{M_{l_2}/M_{l_1}}$, equal to 4.7 for H_2/CO_2, and generally uninteresting for most practical gas separations (in the remainder of this text we refer to this type of separation behavior loosely as "$M^{-1/2}$ separation"). A typical micropore mechanism, as described, dominated by concentration and mobility may lead to much more interesting separation mechanisms. Correlation effects, for example, can be particularly strong for $\theta \rightarrow 1$ and in single-file diffusion where larger molecules cannot pass each other inside the pore.

4.3. Gas- and Liquid-Phase Transport by the Viscous Flow

Transport of liquids in meso- and macropores occurs entirely by the *viscous flow mechanism*, driven by a mechanical pressure difference. The (convective) mass transport is the direct result of the development of a velocity distribution in the fluid continuum. Viscous transport in membrane pores is generally calculated from the Hagen–Poiseuille equation for stationary Newtonian flow in a cylindrical capillary. For practical membranes this leads to the following expressions for the permeance of gases and liquids:

$$f_l^{\text{vf}} \approx \frac{\phi_\text{p} \varnothing_\text{p}^2}{32\tau_\text{p} X \eta_l \mathrm{R}T} \frac{\bar{p}_l}{}; \quad \bar{p}_l = \frac{p_{l,\text{f}} + p_{l,\text{p}}}{2} \tag{5}$$

$$f_\ell = \frac{\phi_\text{p} \varnothing_\text{p}^2}{32\tau X} \tag{6}$$

These expressions assume that the velocity of the liquid is zero at, and parallel to, the pore wall. Viscous flow is nonseparative for molecules. However, the flow field around particles, smaller than $\varnothing_\text{p}$, near the pore entrance may lead to a certain extent of size exclusion. Mesoporous membranes that have a charged pore surface in salt solutions may exhibit significant ion retention by a space charge effect if $\varnothing_\text{p}$ is smaller than the Debye length of the solution.[6] Viscous flow expressions such as Equations (5) and (6) are often used to calculate the flow resistance in macroporous filters and membrane support structures. For liquids in small mesopores, a correction may be necessary for the occurrence of a <1 nm thin immobile layer near the wall.

5. Discussion

Verweij et al.[7] provided a number of interrelated generic "stretch goals" for inorganic membranes as follows:

1) $f_{l_1}^{tot} > 10^{-5}\,\text{mol}\,\text{m}^{-2}\,\text{s}^{-1}\,\text{Pa}^{-1}$ and $\alpha_{l_1,l_2}^{tot} > 100$; $f_l^{tot} > 10^{-12}\,\text{mol}\,\text{m}^{-2}\,\text{s}^{-1}\,\text{Pa}^{-1}$, and $R_l > 99\,\%$.
2) $<50\,\%$ change in these properties over $>10\,000$ h operation with >10 start/stop cycles.
3) Regeneration and/or in situ repair capability to restore $>90\,\%$ of the original transport properties after degradation.
4) Manufacturing yield $>90\,\%$ with zero hours transport properties, reproducible within $10\,\%$.
5) Membrane surface per volume $>100\,\text{m}^2\,\text{m}^{-3}$.
6) Cost $<\text{US\$}\,500\,\text{m}^{-2}$.

The DWNT membranes of Holt et al.[1] will easily meet and exceed the generic stretch goal 1 for permeance. In addition they likely meet goals 2–5. The cost goal 6 is a very crude estimate and the actual benchmark value is strongly correlated with other performance parameters. It can only be established and verified in a complete system integration and optimization study for which all membrane parameters must be well known. The $<\text{US\$}500\,\text{m}^{-2}$ may not be met by the current small-scale manufacturing process, but might be approached by the application of cheaper substrates, and well-chosen manufacturing routes that make use of self-organization methods.

At this point it is unclear to what extent the DWNT membrane will meet practical selectivity goals. Holt et al.[1] showed that their membranes are virtually gas and liquid dense until the caps are etched open. This indicated that

there are no major processing defects introduced in the early processing stages. In addition, they demonstrated an impressive size exclusion for their membranes by showing the permeation of a 1.3 nm $[Ru(bpy)_3]^{2+}$ complex while >2-nm-diameter Au particles were perfectly blocked. This confirmed:

- the 1.6 nm pore diameter, $Ø_p$, observed with TEM,
- that many of the nanotubes were open on both sides,
- and that there are no *membrane defects* with $Ø_p \gg 2$ nm.

The DWNTs are borderline microporous with $Ø_p = 1.3$–2 nm and a description in terms of occupied and empty sites is questionable considering the very smooth nature of the inner nanotube surface. The data for the hydrocarbons show some evidence for sorption effects as they occur in micropores.

5.1. Gas Transport: $M^{-1/2}$ May Not Mean Knudsen

The DWNTs are also borderline mesoporous with $Ø_p =$ 1.3–2 nm so that a description in terms of a Knudsen mechanism is as questionable as the micropore hopping description. To apply Equation (4) for the DWNT membranes:

- $\phi_p < 0.005$ is obtained by multiplying the reported pore density ($< 25 \times 10^{18}\ m^{-2}$) by the pore cross section, $\pi \cdot (8 \times 10^{-10})^2\ m^2$.
- $\tau = 1$ due to the straight channel geometry.

State-of-the-art mesoporous membranes, obtained by colloidal packing of nanoparticles, have $\phi_p \approx 0.35$ and $\tau \approx 3$,[8] which leads to a difference in ϕ_p/τ of >20 and hence f_l^{Kn} in favor of the colloidal packing structures. It can be expected, however, that this difference can become smaller with a more densely packed arrangement of nanotubes. On the other hand, Holt et al.[1] report an enhancement of 16–160 of their gas permeance over the calculated Knudsen value. This enhancement may lead, for very thin membranes, to the situation that molecular transport in the tubes is no longer rate-limiting. The "ballistic" flux of molecules that arrive from the external gas phase can be estimated as

$$j_{gas}^{Bal} = \left(\frac{\Delta p_{gas}}{\sqrt{2\pi R T M_{gas}}} \right) \tag{7}$$

so that the ratio between the ballistic surface flux and the Knudsen flux becomes

$$j_{gas}^{Bal} / j_{gas}^{Kn} < \frac{3X}{4Ø_p} \tag{8}$$

in which the "<" sign in Equation (8) accounts for a less than 100% capture efficiency. For the DWNT membranes, Equation (8) yields a value of 938, which is roughly one order of magnitude different from the reported enhancement factors.[1] A simple ballistic capturing mechanism implies that separation factors are either infinite for size exclusion or equal to the "Knudsen" square root of mass ratio. The latter is fairly uninteresting for most separations. The DWNT membranes of Holt et al.[1] show predominantly square-root mass ratio separation factors but, as shown in Section 5.1., this provides no direct support for either a Knudsen or a ballistic mechanism.

The unique gas permeation properties of the DWNT membranes[1] stem from the very weak interaction between the gas molecules and the tube wall when the molecule translates in the axial (z) direction. Skoulidas et al.[9] showed that the potential energy barrier, u^z, for axial translation of CH_4 inside a (10,10) single-walled carbon nanotube (SWNT) is only $6 \times 10^{-4}\ eV = 0.02 k_B T_{room}$, whereas in zeolite ZSM-12 micropores, $u^z = 0.045\ eV = 1.7 k_B T_{room}$. This has a profound impact on the dynamics of gas molecules. To the first approximation, CNTs can be thought of presenting a smooth, attractive surface (binding energy u^{bind} on the order 10^{-1} eV)[10] to the gas molecules, whereas zeolite micropore channels present a rough, attractive surface. The Knudsen transport mechanism is somewhat physically feasible in the zeolite channels, but not at all possible in CNTs as was already suggested by Holt et al.[1] Due to the high specularity (Maxwell coefficient $\ll 1$)[11] of NT/molecule collisions, the mean free path of the gas molecule (persistence length of its velocity autocorrelation function), at least in the z-direction, is not mainly governed by the channel diameter Ø. In the classical picture of fully specular transport of a particle in a tube, there is not even an effect of Ø.

In pure, non-hydrocarbon gas-permeation experiments (H_2, He, Ne, N_2, O_2, Ar, CO_2, Xe), Holt et al. found an $M^{-1/2}$ dependence in the permeability,[1] that is, light gases diffuse faster, in proportion to the molecule's thermal velocity $v \propto (k_B T/M)^{1/2}$. The $M^{-1/2}$ dependence is often associated with Knudsen diffusion for the following reason: The self-diffusion coefficient, D^s, of a gas molecule is simply $v\lambda$, where λ is its mean free path. Thus, the $M^{-1/2}$ permeability could be explained if one assumes:

1) the gas molecule mean free path is according to Knudsen: $\lambda \approx Ø$, a gas-species-independent constant,
2) the permeability is somehow proportional to D^s in a very simple fashion.

Experimentally, the problem with the above Knudsen diffusion interpretation is that the magnitude does not work out for DWNT membranes. The measured absolute permeability is larger than the Knudsen formula by a factor of 10^1–10^2,[1] and thus the name "fast mass transport". The above assumptions 1) and 2) were also shown to be flawed by the molecular dynamics (MD) simulations of Skoulidas, Johnson, and Sholl et al.,[9,12,13] before experimental results were available. The true story of gas transport in CNTs and the $M^{-1/2}$ dependence could be considerably more complicated than the simple Knudsen picture.

Figure 2a shows MD simulation trajectories of CO_2 molecules in a (40,40) SWNT at 298 K, and Figure 2b shows their density profiles at different external pressures (1–

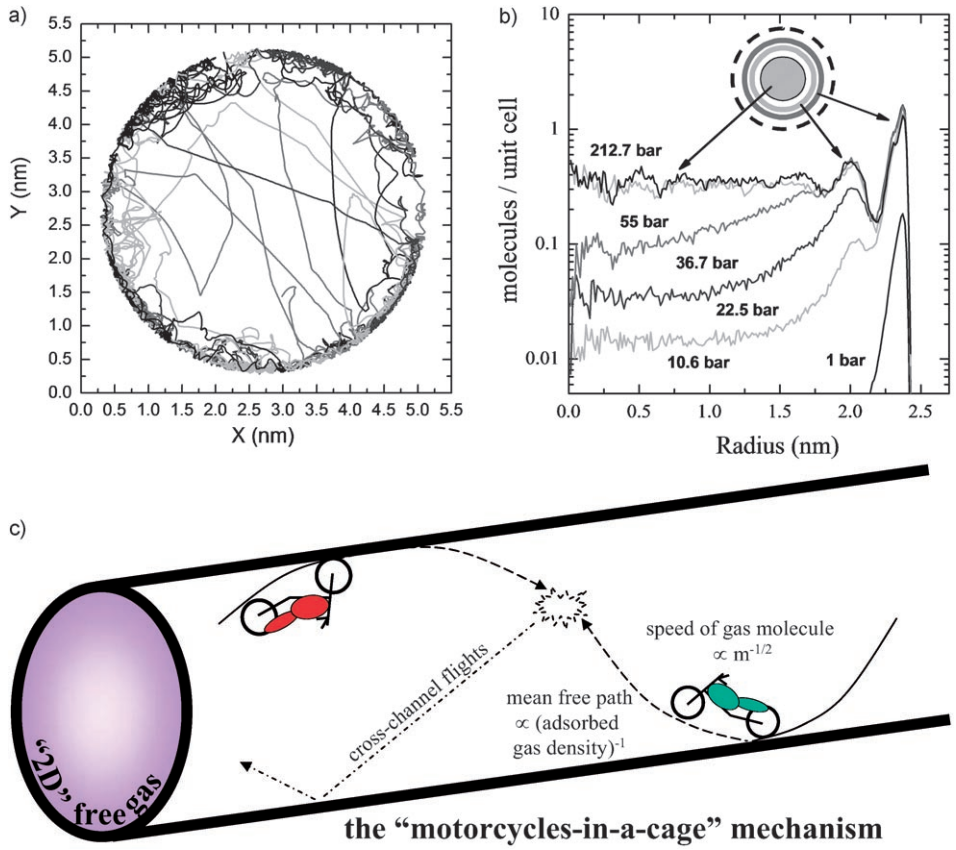

Figure 2. a) Molecular dynamics simulation trajectories of CO_2 molecules in a (40,40) SWNT at 298 K and an external partial pressure of 1 bar; b) simulated density profiles of CO_2 inside a (40,40) SWNT as a function of the external gas pressure. One unit cell has an axial length of 2.5 Å and consists of 160 carbon atoms (adapted from Ref.[12] with permission); c) cartoon of the "2D free gas" model, drawing an analogy to running motorcycle gangs inside a cylindrical cage. The motorcycles run *on* the cage most of the time, collide with other motorcycles frequently *near* the cage, but occasionally send one flying *across* the channel. The CNT/CO_2 interaction is such that the cage has low friction and high specularity in collision with the motorcycles.

10 bar is industrially the most relevant). Clearly, there is a strong enhancement of gas density near the NT walls. It is useful to regard a certain ideal limit of such gaseous system as a "2D free gas". By "2D", we mean in the sense of the earth's atmosphere: it is really 3D, but there is a gradient, and it wraps around. By "free", we mean the friction between the gas and the NT is small: u^z is tiny compared to the kinetic energy of the molecule, and is insufficient to affect its z-momentum quickly.[11] What does mainly affect its z-momentum is collision with other adsorbed molecules in the same "2D free gas".

Figure 2c illustrates the "2D free gas" ideal limit as running a motorcycle gang inside a cylindrical cage. The cage provides centrifugal force support, but cannot slow down the motorcycles quickly. The axial mean free path λ of a motorcycle, instead of limited as $\approx \emptyset_p$ as in the Knudsen diffusion model, depends on the adsorbed gas density. When two motorcycles collide, most often both stay near the cage wall after the collision.[12] Occasionally, the collision sends a motorcycle into a cross-channel flight. Both modes of motion (near-cage spiraling and cross-channel "ping pong") would have an axial mean free path proportional to $1/C_{ad}\sigma$, where C_{ad} is the peak internal density in Figure 2b, and σ is the collisional cross section (in units of m^2) as in the kinetic theory of gases. Thus the self-diffusivity of the "2D free gas" model

$$D^s \approx \left(\frac{k_B T}{M}\right)^{1/2} (C_{ad}\sigma)^{-1} \quad (9)$$

would be rather similar in form to the 3D free gas if one just replaces the density of the 3D gas by C_{ad}.

From the MD simulations,[9,12,13] the self-diffusivity D^s has been shown to depend sensitively on C_{ad} as the model Equation (9) would indicate. But the simulations of Sholl et al. also revealed another side to the story. The chemical diffusion coefficient, $\tilde{D}$, has been found to be virtually independent of C_{ad}.[9,12,13] This amazing constancy of $\tilde{D}$ was already found for single-component microporous hopping diffusion,[5] as well as in molecular dynamics simulations of single-file diffusion in very narrow pores.[14,15] In this case it follows from a cancellation of concentration-dependant terms in the product of the thermodynamic factor $\partial \log F/\partial \log C_{ad}$ and the mobility. The gas fugacity, F (a measure of the chemical potential), blows up at large C_{ad} due to steric repulsions between the adsorbed gas molecules.[16] On the other hand, we postulate that the mobility might have roughly $1/C_{ad}$ dependence as the "2D free gas" model would suggest for the mean free path. If we assume an adsorption thermodynamics model $\Delta\mu/k_B T = \Delta \log F = \Delta C_{ad}\Omega_{ex}$ where Ω_{ex} is a sterically excluded constant volume of molecular dimensions, $\partial \log F/\partial \log C_{ad}$ would be proportional to C_{ad}, which would cancel with the $1/C_{ad}$ dependence in mobility exactly, causing $\tilde{D}$ to be nearly a constant.

From above, we see that the ultra-smoothness of the potential energy landscape for axial translation has a profound impact on the overall transport properties of a confined gas. Fundamentally, this is due to two features of the CNT: Structurally, the atomic planarity of graphene at 0 K, and chemically, the nonpolar nature of the carbon network. Zeolites and other ceramic membranes, which have charged groups on the pore surface and can polarize the gas molecules, apparently induce a much larger u^z, and therefore

belong to a different class. It has been demonstrated that thermal fluctuations of the NT do not significantly alter its gas transport behavior above 1 bar at room temperature.[17]

Up to now we have been addressing pure gas permeability. Despite the undoubtedly fast transport in DWNT membranes—with diffusivity of the same order as that of the free gas ($\tilde{D} \approx 10^{-5}\ m^2 s^{-1}$)—whether these membranes could find industrial applications depends a lot on whether they could beat the $M^{-1/2}$ selectivity to comply with the selectivity stretch goals. Here again, MD simulations have provided valuable insights. Chen and Sholl have computed both the diagonal and off-diagonal components of the Onsager transport coefficient matrix for CH_4/H_2 binary gases.[13,18] We make two observations based on their results: a) the off-diagonal transport coefficient is of similar magnitude as the diagonal coefficients, indicating significant translational correlation between the motions of the two species. This can be expected if we consider two motorcycle gangs, the red and the green, running in the same cylinder cage. Red–green collisions are unavoidable and must be highly correlated with red–red and green–green collisions (chain collisions), due to the slow dephasing action of the cage wall. In other words, effects of a collision persist for a long time. b) Having said that, selectivity in excess of $M^{-1/2}$ in such multicomponent permeations seems to be largely governed by the adsorption thermodynamics, rather than the kinetics. Assuming both red and green motorcycles have similar collisional cross sections (which usually cannot vary greatly), the mean free path of a red motorcycle would be *always* similar in magnitude to that of a green motorcycle, $\lambda_{red} \approx \lambda_{green} \propto 1/(C_{ad,red}+C_{ad,green})$. But, if the binding energy is favorable to the red, the cage surface is preferably the red gang's "turf", and there will be a lot more red motorcycles running around, marginalizing the green who cannot find adsorption sites, for a fixed ratio of outside gas fugacities. Thus, the flux of the red motorcycles could overwhelm that of the green motorcycles, comparable to what happens for type 2 microporous separation.

To achieve the selectivity target of >100, this argument would require, by a rough estimate, a binding energy difference $\Delta u^{bind} \approx \ln(100) k_B T \approx 0.1$ eV between the two adsorbed gas species A and B. This might be challenging for most binary gas combinations. Perhaps with boron nitride nanotubes or chemical functionalization of carbon nanotubes, Δu^{bind} can be tuned, but one must also keep u^z small in order to maintain fast gas transport. Another idea would be to use a third gas adsorbate C, which has strong lateral interactions with A, but not with B, so as to bias the effective binding energies of A and B.

5.2. Water Transport: Breakdown of the Poiseuille Flow

The use of Equation (7) to estimate the viscous flow resistance of water in DWNTs leads to similar concerns for the small ϕ_p/τ values as was mentioned for Knudsen transport. However, also in this case, there is a significant enhancement of permeance, this time, over the Hagen–Poiseuille value by a factor of 560–8400. This effect is ascribed to the occurrence of significant slip and hence, nonzero velocity of water at the pore walls. The occurrence of slip is explained once more by the very smooth pore walls and the fact that the water molecules have little affinity for the hydrophobic nanotubes. Holt et al. were well aware that the typical continuum concept of viscous flow is not easily applicable to 1.6-nm-diameter pores. However, the large enhancement factors demonstrate that the water transport is fast regardless. The viscous flow stick/nonstick concept completely loses its meaning for micropores and gas transport in the Knudsen regime. As an example, efficient water transport is also well documented for thin zeolite A membranes which have $0.4 < Ø_p < 0.5$ nm. In such membranes, the water molecules just fit inside the pore and apparently have significant mobility with respect to the pore wall. Representative data are provided elsewhere for separation of water from mixtures with ethanol by pervaporation (liquid at the feed side, vapor at the permeate side).[19] The best performance currently reported is for a 10-μm-thick membrane on a porous mullite support: $j_{H_2O} = 0.13\ mol\,m^{-2}s^{-1}$ with $\alpha_{H_2O/C_2H_5OH} = 47\,000$ for 10% water in the feed at 120 °C. For the 2-μm-thick membrane DWNT 1, mentioned in Table 2, the enhanced pure $j_{H_2O} = 7$–$39\ mol\,m^{-2}s^{-1}$ at $\Delta p = 10^5$ Pa and 120 °C.[1] This shows, once more, the impressive effect of slip-enhancement. The DWNTs liquid-phase transport, however, has not been demonstrated to be separative when the molecule sizes are both smaller than Ø. A comparison in terms of separation performance, simply taken as $j_{H_2O} \times \alpha_{H_2O/C_2H_5OH}$, yields $5850\ mol\,m^{-2}s^{-1}$ for the zeolite membranes and likewise 7–$39\ mol\,m^{-2}s^{-1}$ for DWNT 1.

Both Majumder et al.[20] and Holt et al.[1] have reported fast water transport across CNT membranes when sandwiched between bulk liquid water at room temperature. These experiments corroborate the earlier MD simulations of Hummer et al.[21,22] The best quantitative interpretation of liquid-phase water transport in DWNTs is probably done through a comprehensive molecular dynamics (MD) treatment. The first question one may ask is, why does water wet CNTs at all? A configuration was created in which water flow though CNTs was driven by an osmotic pressure difference.[22] The study showed that water flow is limited mainly by particle entry and exit events, and that tube length had hardly any effect. For the (6,6) SWNT studied by Hummer et al., its tube diameter (0.8 nm) is so narrow that only a single water molecule could be inserted, forming a single-file water chain. According to Truskett et al.,[23] the hydrophobic confining wall reduces the average number of favorable fluid–fluid interactions per molecule; it disrupts the hydrogen-bonding pattern in the fluid.[24] Inside the SWNT two hydrogen bonds are lost per molecule compared to bulk liquid water, costing it approximately $+0.4$ eV in binding energy. This is only partially recuperated from the van der Waals interaction with the CNT wall (approximately -0.17 eV), making the inserted molecule approximately $+0.2$ eV unfavorable in the average binding energy, as indicated by the vertical arrows in Figure 3a.

However, a water chain did form in the simulation (Figure 3b). This turns out to be due to a subtle statistical effect at finite temperature. Hummer et al. noted that while the

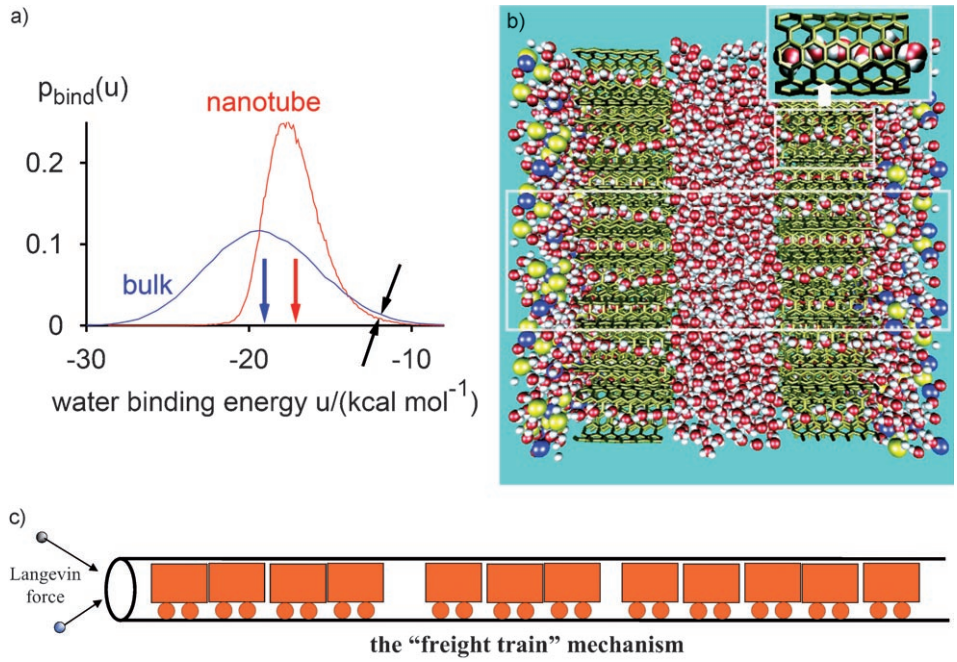

Figure 3. a) Distribution of water binding energies in bulk liquid water (blue) and inside the nanotube (red) at 300 K (adapted from Ref.[21] with permission); b) MD snapshot of pure water separated from a salt solution by two membranes of hexagonally packed SWNTs (blue: Na^+; yellow: Cl^-; red: O; white: H). Inset shows an enlarged image of a SWNT filled with a hydrogen-bonded water wire (adapted from Ref.[22] with permission); c) illustration of the single-file diffusion of water inside a SWNT.

average of the binding energy distribution (Figure 3a) has shifted up, its width has become narrower. Because of this, there are less very-high-energy water molecules, as indicated by slanted arrows in the Figure 3a distribution. These very-high-energy molecules play a disproportionally large role in the statistical mechanics equation for the chemical potential, such that after averaging, the H_2O molecules in the tube are actually better off in chemical potential by -0.04 eV than the bulk liquid. If we liken the very-high-energy molecules to troublemakers in a group of school children, then the constraining effect of the NT eliminates the troublemakers, and results in making everyone just a bit happier.

The water molecules confined in a (6,6) SWNT still have considerable entropy at 300 K: The hydrogen bonds, which are nearly aligned to the nanotube axis, have a lifetime of 5.6 ps, and the water molecules can freely rotate about that axis.[21] But clearly, the water chain cannot be considered "liquid water" in any traditional sense of the term. In the classic Poiseuille flow model with a no-slip boundary condition, the dissipation rate comes entirely from the transverse momentum transfer inside the liquid, proportional to the bulk liquid viscosity. Here, however, one may expect the dissipation rate to originate entirely from water chain/NT friction, instead of water–water momentum transfer. Hummer et al. further noted that this wall friction appears to be exceedingly small,[21] as in the gas-diffusion case.

Indeed, graphite is an industrial-grade solid lubricant. Recently, it has been verified to have the so-called "superlubricity" property from scanning probe experiments on solid–solid contacts.[25] The idea is that since the graphene plane is atomically flat and very rigid, any large solid structure that has incommensurate contact has a very low (in an ideal limit, zero) friction coefficient. The relative translation of the two rigid bodies involves, simultaneously, equal numbers of bonds to break as to reform, and therefore requires only zero total potential energy fluctuation per unit contact area. The water chain here is not very rigid and it may not be considered as a true "solid", but it is tempting to draw the analogy of the water chain in CNTs to freight cars on rails, as shown in Figure 3c. The freight cars are pushed on both terminals by Langevin thermal forces, which average to the pressures. The cars do not necessarily form one long contiguous train terminal-to-terminal; they could break up and recombine into new trains inside at any time.

Abnormalities in the structure and dynamics of water inside sub-2 nm CNTs are often reported.[26,27] These are the kinds of tubes that Holt et al.[1] exploited in their water-permeation experiments. There is really no physical basis to apply the Poiseuille flow equation, which uses the bulk liquid viscosity, onto these systems. One could try to modify the Poiseuille flow model to include boundary slip, by introducing a new parameter called the slip length R_{slip}, which is the ratio of the translational velocity at the wall, v_z, to the characteristic velocity gradient in the transverse direction, $\partial_y v_z$: $R_{slip} = v_z/(\partial_y v_z)$. The problem is that in order to fit the experimental data, Holt et al. found they must use a slip length of the order 100 nm! This is 100× larger than the tube diameter itself, which means 99% of the velocity drop occurs between the water body and the NT wall, and only 1% of the velocity drop occurs inside the water. If we take this model to be literally true, this is just another way of saying that the water moves like a solid! The key assertion of the Poiseuille flow picture is that water–water momentum transfer is a main component of the total dissipation. It is likely that this defining characteristic has broken down for the smaller CNTs. The water–NT friction has become of paramount importance.

Majumder et al. used MWNTs with $Ø_p = 7$ nm; for these larger tubes, one can expect the water body inside to behave pretty much like bulk liquid water. It has been shown with molecular dynamics simulations that at this length scale, which is >10 times larger than the molecular dimension, the Poiseuille flow equation may work really well,[28] if the friction between the wall and the fluid is large such that no slip occurs. This could be the case if the inter-

action potential between the wall and the fluid atoms is strong, and they have similar length scales (σ parameter in Lennard–Jones potentials).[28] But this does not seem to be the case from experimental data. Majumder et al. reported slip lengths that are 10^4 times larger than $Ø_p$.[20] Instead of *flowing*, the water body is really *translating*, as the Figure 3c cartoon illustrates. This slug flow behavior would be the case even if the confined water behaves thermodynamically as the bulk water, as long as the water-NT friction is low enough.[11]

6. Conclusions

Holt et al.[1] have demonstrated an impressive capability to produce dense parallel arrangements of double-walled carbon nanotubes with both sides open in a supported membrane structure. To realize this highly perfect geometry they make extensive use of advanced microfabrication facilities. The membranes have a characteristic $Ø_p$ of 1.6 nm with an estimated effective pore density $\phi_p < 0.005$. Gas- and liquid-transport measurements show substantial flow enhancements of 16–160 with respect to real Knudsen gas diffusion and 560–8400 with respect to nonslip Hagen–Poiseuille viscous flow. Alternative transport mechanisms have been proposed that emphasize transfer limitations at the tube entrance. In any case, the very efficient transport in the tubes make that the kinetics of surface transfer becomes more important. If they become dominant, the separation factors for this type of membrane will be either infinite in case of true size exclusion, close to unity for gas diffusion, and exactly 1 for simple liquid mixtures.

We see that none of the classic models for gas (Knudsen) and water (Poiseuille) transport work in a meaningful way for CNT membranes. This is ultimately caused by the ultralow friction of CNT walls with molecules. CNTs are somewhat unique in this aspect due to the true atomic planarity and high rigidity of the graphene plane, and the nonpolar nature of the sp^2 carbon network, which distinguishes them from other ceramic membrane systems that also have atomic-scale narrow pores. Despite the undoubtedly fast mass transport for both gas and water, how to enhance the selectivity of CNT membranes is a big challenge for both the experimentalists and modelers.

The DWNT membranes may not be sufficiently cost effective for large-scale applications but might be deployed for the separation of valuable molecular entities by size exclusion. In addition, the DWNTs form an ideal test bed for testing gas- and liquid-phase transport theories. The road to useful industrial applications of CNT membranes may be a long and arduous one, due to the selectivity and cost requirements. Fortunately, atomistic simulations can really provide some help and guidance. More conclusive evidence for the actual and possible separation mechanisms in the DWNT membranes will be obtained from the interpretation of actual separations for a wide range of compositions and circumstances.

[1] J. K. Holt, H. G. Park, Y. Wang, M. Stadermann, A. B. Artyukhin, C. P. Grigoropoulos, A. Noy, O. Bakajin, *Science* **2006**, *312*, 1034 – 1037 (and online supporting material).
[2] R. M. de Vos, H. Verweij, *Science* **1998**, *279*, 1710 – 1711.
[3] J. K. Holt, A. Noy, T. Huser, D. Eaglesham, O. Bakajin, *Nano Lett.* **2004**, *4*, 2245 – 2250.
[4] W. J. Koros, Y. H. Ma, T. Shimidzu, *Pure Appl. Chem.* **1996**, *68*, 1479 – 1489.
[5] H. Verweij, *J. Mater. Sci.* **2003**, *38*, 4677 – 4695.
[6] W. B. S. de Lint, N. E. Benes, *J. Membr. Sci.* **2004**, *243*, 365 – 377.
[7] H. Verweij, Y. S. Lin, J. H. Dong, *Mater. Res. Soc. Bull.* **2006**, *31*, 756 – 764.
[8] M. L. Mottern, J. Y. Shi, K. Shqau, D. Yu, H. Verweij in *Membranes: Manufacturing and Applications* (Eds.: N. N. Li, A. G. Fane, W. S. W. Ho, T. Matsuura), Wiley, New York, **2006**, in press.
[9] A. I. Skoulidas, D. M. Ackerman, J. K. Johnson, D. S. Sholl, *Phys. Rev. Lett.* **2002**, *89*, 185901.
[10] J. Li, T. Furuta, H. Goto, T. Ohashi, Y. Fujiwara, S. Yip, *J. Chem. Phys.* **2003**, *119*, 2376 – 2385.
[11] S. K. Bhatia, H. B. Chen, D. S. Sholl, *Mol. Simul.* **2005**, *31*, 643 – 649.
[12] A. I. Skoulidas, D. S. Sholl, J. K. Johnson, *J. Chem. Phys.* **2006**, *124*, 054708.
[13] H. B. Chen, D. S. Sholl, *J. Membr. Sci.* **2006**, *269*, 152 – 160.
[14] O. G. Jepps, S. K. Bhatia, D. J. Searles, *Phys. Rev. Lett.* **2003**, *91*, 126102.
[15] S. K. Bhatia, O. G. Jepps, D. Nicholson, *J. Chem. Phys.* **2004**, *120*, 4472.
[16] E. J. Maginn, A. T. Bell, D. N. Theodorou, *J. Phys. Chem.* **1993**, *97*, 4173 – 4181.
[17] H. B. Chen, J. K. Johnson, D. S. Sholl, *J. Phys. Chem. B* **2006**, *110*, 1971 – 1975.
[18] H. B. Chen, D. S. Sholl, *J. Am. Chem. Soc.* **2004**, *126*, 7778 – 7779.
[19] M. Kondo, M. Komori, H. Kita, K. Okamoto, *J. Membr. Sci.* **1997**, *133*, 133 – 141.
[20] M. Majumder, N. Chopra, R. Andrews, B. J. Hinds, *Nature* **2005**, *438*, 44; Erratum: *Nature* **2005**, *438*, 930.
[21] G. Hummer, J. C. Rasaiah, J. P. Noworyta, *Nature* **2001**, *414*, 188 – 190.
[22] A. Kalra, S. Garde, G. Hummer, *Proc. Natl. Acad. Sci. USA* **2003**, *100*, 10175 – 10180.
[23] T. M. Truskett, P. G. Debenedetti, S. Torquato, *J. Chem. Phys.* **2001**, *114*, 2401 – 2418.
[24] D. S. Sholl, J. K. Johnson, *Science* **2006**, *312*, 1003 – 1004.
[25] M. Dienwiebel, G. S. Verhoeven, N. Pradeep, J. W. M. Frenken, J. A. Heimberg, H. W. Zandbergen, *Phys. Rev. Lett.* **2004**, *92*, 126101.
[26] K. Koga, G. T. Gao, H. Tanaka, X. C. Zeng, *Nature* **2001**, *412*, 802 – 805.
[27] A. I. Kolesnikov, J. M. Zanotti, C. K. Loong, P. Thiyagarajan, A. P. Moravsky, R. O. Loutfy, C. J. Burnham, *Phys. Rev. Lett.* **2004**, *93*, 035503.
[28] J. Li, D. Y. Liao, S. Yip, *Phys. Rev. E* **1998**, *57*, 7259 – 7267.

Received: May 25, 2007
Revised: July 4, 2007
Published online on November 16, 2007

